



Metal microparticle – Polymer composites as printable, bio/eco-resorbable conductive inks

Seungae Lee¹, Jahyun Koo¹, Seung-Kyun Kang², Gayoung Park³, Yung Jong Lee⁴, Yu-Yu Chen⁵, Seon Ah Lim⁶, Kyung-Mi Lee⁶, John A. Rogers^{7,*}

¹ Department of Materials Science and Engineering, Northwestern University, Evanston, IL 60208, USA

² Department of Bio and Brain Engineering, Korea Advanced Institute of Science and Technology (KAIST), Daejeon 34141, Republic of Korea

³ Global Research Laboratory, Department of Biochemistry and Molecular Biology, Department of Biochemistry & Molecular Biology and Division of Brain Korea 21, Korea University College of Medicine, Seoul 02841, Republic of Korea

⁴ Department of Materials Science and Engineering, Korea Advanced Institute of Science and Technology (KAIST), Daejeon 34141, Republic of Korea

⁵ Frederick Seitz Materials Research Laboratory, University of Illinois at Urbana-Champaign, Urbana, IL 61801, USA

⁶ Global Research Laboratory, Department of Biochemistry and Molecular Biology, Korea University College of Medicine, Seoul 02841, Republic of Korea

⁷ Center for Bio-Integrated Electronics, Department of Materials Science and Engineering, Biomedical Engineering, Chemistry, Mechanical Engineering, Electrical Engineering and Computer Science, and Neurological Surgery, Simpson Querrey Institute for Nano/Biotechnology, McCormick School of Engineering and Feinberg School of Medicine, Northwestern University, Evanston, IL 60208, USA

Biologically and environmentally resorbable electronic devices support application possibilities that cannot be addressed with conventional technologies. This paper presents highly conductive, water-soluble composites that can be printed to form contacts, interconnects, antennas, and other important features that are essential to nearly all systems of this type. An optimized material formulation involves *in situ* polymerization to yield a polyanhydride containing a dispersion of molybdenum microparticles at appropriate concentrations. Comparisons of essential physical and electrical properties of these materials to those of composites formed with other polymers and other metal microparticles reveal the relevant considerations. Various functional demonstrations of screen-printed test structures and devices illustrate the suitability of these conductive inks for use in water-soluble electronic devices. A key advantage of the material introduced here compared to alternatives is its ability to maintain conductance over significant periods of time while immersed in relevant aqueous solutions. Studies involving live animal models establish the biocompatibility.

Introduction

Electronic systems constructed with materials that dissolve in biofluids and/or ground water represent an important type of transient device technology, of particular interest in biomedical implants that provide function over relevant timeframes and then disappear without the need for secondary surgeries [1–5]. Such systems can also serve as ‘green’ forms of electronics, capable of naturally resorbing into the environment without haz-

ardous waste streams [6–9]. Recent research establishes many of the foundational materials for such technologies, with demonstrated capabilities in power supply [10,11], wireless data communication [12], energy harvesting [13], and multimodal sensing and actuation [14,15]. One area of continuing interest is in conductive materials for these systems that can be printed at sufficient thicknesses to enable non-planar interconnects, low-loss antennas, and other features for circuit boards, radio frequency identification tags, and other platforms. Previous reports describe composites of hydrophilic polymers, such as polyvinylpyrrolidone (PVP) and poly(ethylene oxide) (PEO), with metal microparticles to yield water-soluble, printable conductors [16,17]. The main disadvantage, however, is that such

* Corresponding author. Fax: +1 (217) 333 2763.

E-mail addresses: Lee, S. (seungae.lee@northwestern.edu), Rogers, J.A. (jrogers@northwestern.edu).

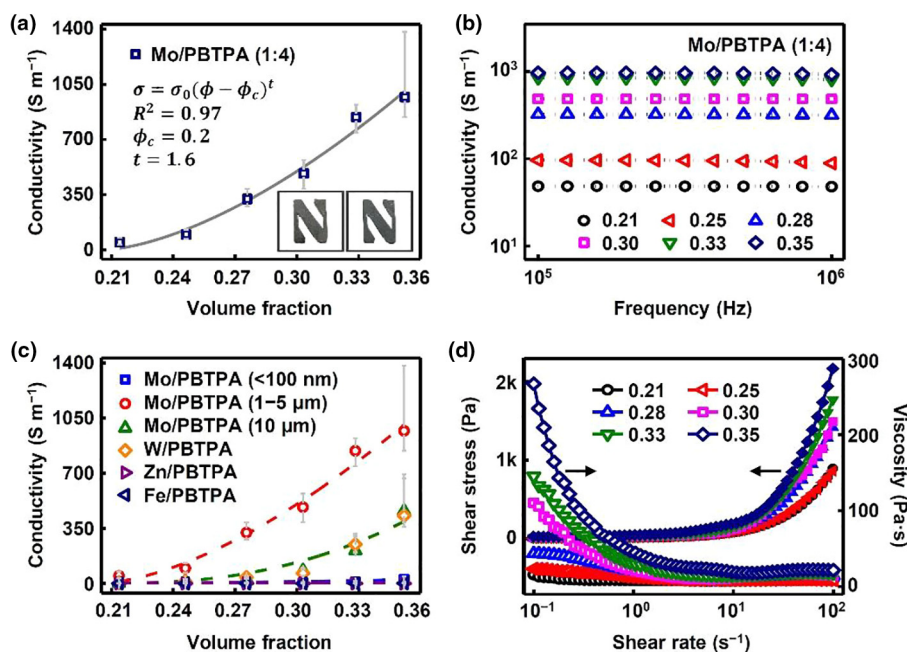


FIGURE 1

Formulations and characteristics of biodegradable conductive pastes. (a) Conductivity of Mo/PBTBA (Poly butanedithiol 1,3,5-triallyl-1,3,5-triazine-2,4,6 (1H,3H,5H)-trione pentenoic anhydride) paste with various volume fractions of Mo microparticles (1–5 μm) in PBTPA, evaluated using direct current (DC) measurement. The inset shows a printed pattern of Mo/PBTBA in an 'N' logo before (left) and after (right) heat treatment. The equation is the percolation scaling law used to estimate the dependence of electrical conductivity of the composite (σ) on the volume fraction of conductive filler, where σ_0 is a scaling factor, ϕ and ϕ_c are the volume fraction and critical volume fraction, respectively, and t is the critical exponent (blue squares are experimental data; the black line is a fit based on the percolation scaling). (b) Conductivity of Mo/PBTBA paste with various volume fractions of Mo microparticles in PBTPA (symbols are the experimental data; dotted lines are fits based on the Drude model), evaluated using alternating current (AC) measurement. (c) Comparison of DC conductivity of Mo microparticle-based paste to pastes made with other kinds of biodegradable metal particles, *i.e.* Mo (<100 nm), Mo (1–5 μm), Mo (<10 μm), W (<10 μm), Zn (<10 μm), and Fe (<10 μm), each in a PBTPA polymer matrix at various volume fraction of metal particles (symbols are the experimental data; dotted lines are fits based on percolation scaling). (d) Shear stress (closed symbol) and viscosity (open symbol) of Mo/PBTBA paste at various volume fractions of Mo microparticle at different shear rates.

materials dissolve on timescales of less than a few days, which is significantly shorter than those of interest for many applications. For instance, previous studies of tungsten (W) composites with PEO show that dissolution occurs within a few minutes after immersion in water, thereby precluding use in most envisioned types of temporary implants [16]. Other reports describe zinc (Zn) composites with PVP that have similar dissolution times, extendable to several hours by the addition of overcoats of poly(lactic-co-glycolic acid) (PLGA) [17].

Here, we describe a transient conductive paste composed of a polyanhydride, as a hydrophobic bioresorbable polymer, that is loaded with molybdenum (Mo) microparticles using a simple process. The resulting material can serve as a printable conductor for water-soluble interconnects, antennas, resistive pressure sensors, and strain gauges. Electrical continuity in representative traces persists for over 9 days of immersion in deionized (DI) water at 37 $^{\circ}C$, thereby greatly exceeding the lifetimes of alternative materials. Tests of biocompatibility in animal models reveal no effects of toxicity.

Results and discussion

The paste uses a matrix of poly butanedithiol 1,3,5-triallyl-1,3,5-triazine-2,4,6(1H,3H,5H)-trione pentenoic anhydride (PBTPA), synthesized by thiol-ene click reactions initiated by exposure to

ultraviolet (UV) light, mixed with Mo microparticles and then thermally cured. A cleavage type photoinitiator, *i.e.* 2,2-dimethoxy-2-phenylacetophenone, induces thiol-ene click reactions with higher efficiency compared to H-abstraction type photoinitiators and thermal initiators [18]. The heating step not only cross-links the regions not completely cured by UV light but also densifies the conductive network through small deformations and shifts in the polymer matrix, as reported previously in different, but related, systems [19–21]. Measurements by differential scanning calorimetry (DSC) (Fig. S1a) indicate that the glass transition temperature (T_g) and the melting temperature (T_m) of this material, which we refer to as Mo/PBTBA paste, are 61 $^{\circ}C$ and *ca.* 168 $^{\circ}C$, respectively. An increase in heat flow appears at ~ 225 $^{\circ}C$, corresponding to the cross-linking reaction. The isothermal curve at 250 $^{\circ}C$ suggests that ~ 20 min is sufficient to cross-link the polymer completely (Fig. S1b). DSC thermograms of the resulting PBTPA (*i.e.* after UV and thermal treatment) show no features, consistent with complete curing (Fig. S1c). Fig. S1d summarizes results of thermogravimetric analysis (TGA), which indicate that the thermal decomposition temperature is higher than 300 $^{\circ}C$.

Fig. 1a shows the direct current (DC) conductivity of the Mo/PBTBA material as a function of volume fraction of Mo microparticles. The fits correspond to expectations based on classical percolation theory, according to

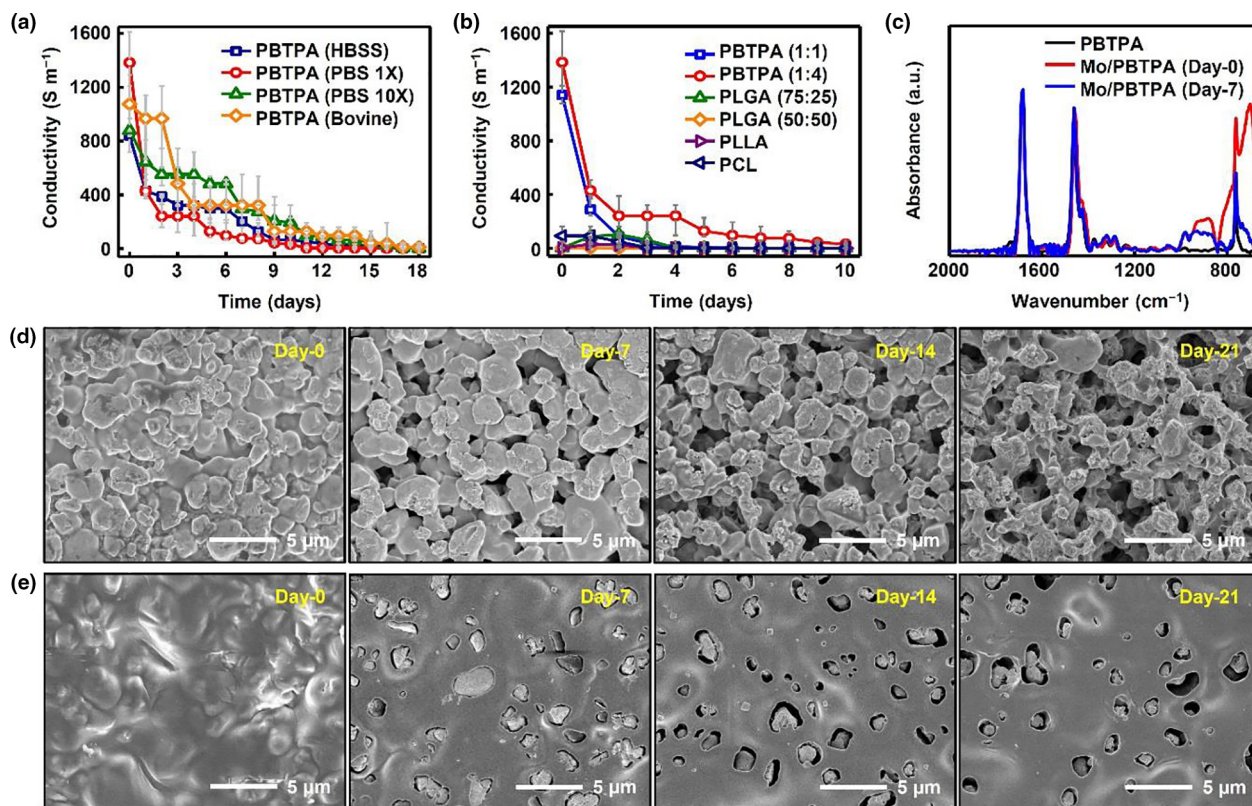


FIGURE 2

Dissolution behavior of conductive Mo/PBTPA paste in phosphate-buffered saline simulated biofluids and bovine serum. (a) DC conductivity of Mo/PBTPA (1:4) as a function of time of immersion in various solutions at 37 °C (blue is Hanks' balanced salt solution (HBSS); red is phosphate-buffered saline (PBS) 1X concentration; green is PBS 10X concentration; orange is bovine serum). (b) DC conductivity of pastes formed with Mo microparticles composited with various biodegradable polymers (35 vol% Mo) as a function of time of immersion in PBS at 37 °C (blue is PBTPA (1:1); red is PBTPA (1:4); green is PLGA (75:25); orange is PLGA (50:50); purple is PLLA; navy is PCL). (c) Infrared absorption spectra of PBTPA (1:4) and Mo/PBTPA paste at different times of immersion in PBS solution at 37 °C. Series of scanning electron microscope (SEM) images of (d) Mo/PBTPA (1:4) paste and (e) Mo/PLGA (72:25) paste at various stage of dissolution in PBS at 37 °C.

$$\sigma = \sigma_0(\phi - \phi_c)^t \quad \text{for } \phi > \phi_c \quad (1)$$

where σ is the conductivity, σ_0 is a scaling factor, ϕ and ϕ_c are the volume fraction and critical volume fraction (percolation threshold), respectively, and t is the critical exponent that defines the dimensionality of the network. The data suggest a critical volume fraction of ~ 0.2 (weight fraction: ~ 0.7) and a critical exponent of ~ 1.6 , the latter of which lies at the lower end of the range expected for three-dimensional systems [22,23].

Fig. 1b presents the alternating current (AC) conductivity of Mo/PBTPA measured across a frequency range from 0.1 to 1 MHz. Increasing the concentration of Mo enhances the conductivity, as expected. The AC conductivity slightly decreases with increasing frequency, indicating metal-like conductive behavior consistent with a Drude model [24–26], where the AC conductivity (σ) is expressed as

$$\sigma(\omega) = \frac{\sigma_0}{1 + \omega^2\tau^2} \quad (2)$$

Here, σ_0 is the DC conductivity, ω is the frequency, and τ is the relaxation time. Fits of the data to this model yield the relaxation time (τ), as listed in Table S1.

Fig. 1c compares the DC conductivity of the Mo/PBTPA material to analogous pastes formed using other bioresorbable metal microparticles and Mo particles with different diameters. Reducing the particle sizes increases the surface area per volume,

thereby enhancing the particle–particle contacts. On the other hand, increasing the sizes reduces the number of contacts needed to form complete conduction pathways. Both the ease of forming contacts and the resistances associated with these contacts can affect the conductivity. Mo/PBTPA pastes with Mo microparticles that have diameters of 1–5 μm show higher conductivity than those with smaller (<100 nm) or larger diameters ($\sim 10 \mu\text{m}$). According to previous studies, the resistance of an isotropic conductive adhesive (ICA) based on a polymer matrix and conductive particles can be defined as $R_c + R_b + R_t$, where R_c is the contact resistance between conductive particles, R_b is the intrinsic resistance of particles, and R_t is the tunneling resistance between two conductive particles [27]. These resistances can be written as

$$R_c = \rho/D \quad (3)$$

$$R_b = \frac{\rho}{\pi d} \ln \frac{d + \sqrt{d^2 - D^2}}{d - \sqrt{d^2 - D^2}} \quad (4)$$

$$R_t = \frac{\rho_t}{\pi(d/2)^2} \quad (5)$$

where ρ is the intrinsic resistivity of conductive filler material, d is a diameter of particles, and ρ_t is the tunneling resistivity between

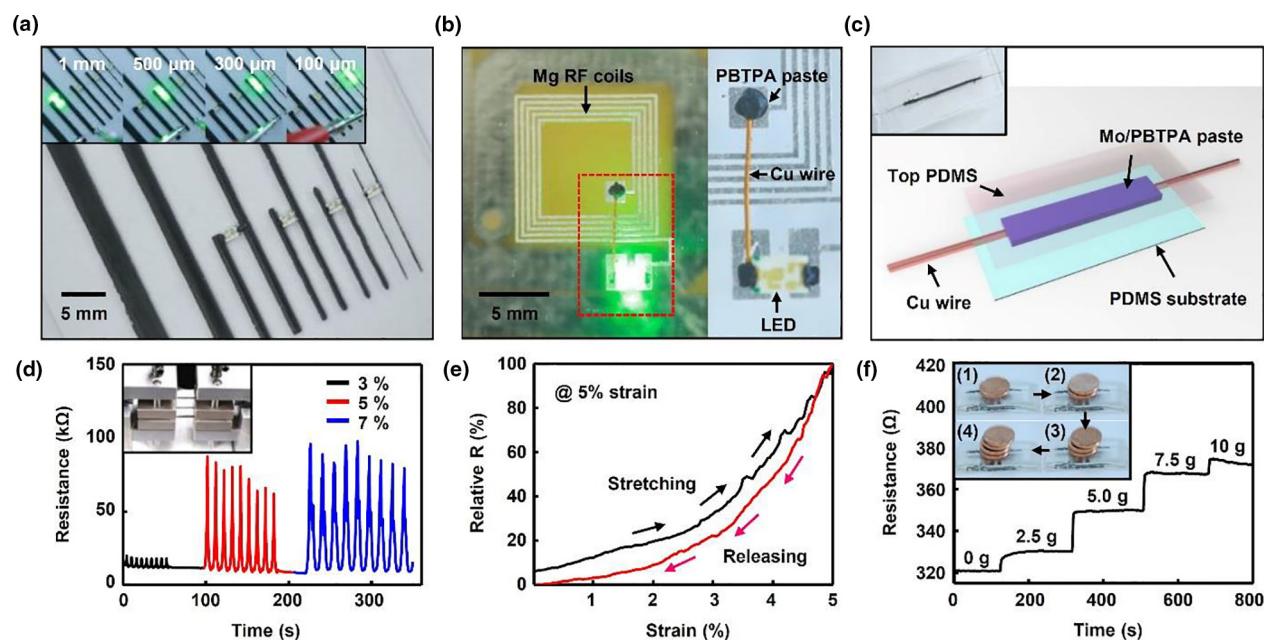


FIGURE 3

Patterning conductive traces of Mo/PBTTPA and integration of them into biodegradable electronic devices. (a) Screen-printed conductive lines of Mo/PBTTPA paste ($100\ \mu\text{m} \sim 3\ \text{mm}$ width, $100\text{-}\mu\text{m}$ thickness) with integrated, small-scale LEDs, after sintering at $250\ ^\circ\text{C}$ on a glass slide. (inset: LEDs activated by applying a voltage of $1.5\ \text{V}$ to the ends of lines of Mo/PBTTPA with widths of $100\ \mu\text{m} \sim 1\ \text{mm}$ and thicknesses of $100\ \mu\text{m}$). (b) Mo/PBTTPA paste used as an interconnect with an RF coil of Mg. Here, a Cu wire electrically joined by Mo/PBTTPA to the start and end points of the coil closes the loop. A primary coil (3 turns of $1\ \text{cm} \times 1\ \text{cm}$ square coil) transfers radio frequency power at $15\ \text{MHz}$ to the secondary coils (Mg RF coils), thereby activating an LED. (c) Schematic diagram of a strain sensor formed with Mo/PBTTPA (inset: image of the device). Screen printing defined the required features of Mo/PBTTPA (2-mm width, 20-mm length, $100\text{-}\mu\text{m}$ thickness) on a flexible substrate (9:1 PDMS, 1.5-mm thickness). Cu wires embedded along 5-mm lengths at the ends of the lines of Mo/PBTTPA served as interfaces for electrical measurements. PDMS ($\sim 200\ \mu\text{m}$ thick) cast on top of the entire device prevented delamination of the Mo/PBTTPA from the substrate during stretching and bending. (d) Cyclic strain test of the sensor at 3%, 5%, and 7% strain. (e) Data from stretching and releasing the sensor at to 5% strain. (f) Pressure sensor constructed with features of Mo/PBTTPA mounted on a curved substrate (9:1 PDMS, 1.5-mm thickness, 150-mm curled radius). The resistance of this Mo/PBTTPA pressure sensor increases with increasing applied force (via addition of coins as test masses).

conductive fillers. D is the contact area between two conductive fillers, according to

$$D = 2\sqrt{\left(\frac{d}{2}\right)^2 - \left(\frac{\pi d/6}{k^2 W}\right)^2} \quad (6)$$

where k is a parameter related to the dimensionality of the ICA, and W is the filler threshold content. The values of k and W can be estimated from percolation theory. Consequently, the total resistance of the paste can be expressed as follows:

$$R = \rho/D + \frac{\rho}{\pi d} \ln \frac{d + \sqrt{d^2 - D^2}}{d - \sqrt{d^2 - D^2}} + \frac{\rho_t}{\pi(d/2)^2} \quad (7)$$

As the sizes of the Mo particles increases, the contact area between particles increases, leading to an increase in the intrinsic resistance and a decrease in both the contact resistance and the tunneling resistance. The equations above suggest that the minimum resistance appears when the particle size is *ca.* $2\ \mu\text{m}$, which is qualitatively consistent with experimental results.

Pastes with iron (Fe) and Zn particles show conductivities lower than those with Mo, likely due to the formation of non-conductive surface oxide layers, consistent with the relative reactivities as defined by their Pauling electronegativity. Since the electronegativities of Zn (1.65) and Fe (1.83) are much lower than those of Mo (2.16) and W (2.36), Fe and Zn tend to form thicker native oxides, resulting in reductions in conductivity of the cor-

responding composites. The formulation with W ($52.8\ \text{n}\Omega\cdot\text{m}$ at $20\ ^\circ\text{C}$) has conductivity similar to that with Mo ($53.4\ \text{n}\Omega\cdot\text{m}$ at $20\ ^\circ\text{C}$) for similar particle diameters (*ca.* $10\ \mu\text{m}$), consistent with their similar reactivity and resistivity. Microparticles of Mo represent a good choice compared to those of other transient metals due to their high conductivity, their resistance to the formation of thick oxides, their broad commercial availability, and their low cost.

The viscoelastic properties of such pastes are important for patterning them by screen printing, where a viscosity in the range of $10\text{--}300\ \text{Pa}\cdot\text{s}$ is typically required. Fig. 1d shows the dependence of the shear stress on shear rate and the viscosity of the Mo/PBTTPA paste as a function of the concentration of Mo. The material exhibits shear-thinning behavior, and a viscosity that increases with the concentration of Mo. When the volume fraction of Mo is 0.35, the viscosity of the Mo/PBTTPA paste is *ca.* $270\ \text{Pa}\cdot\text{s}$ at a shear rate of $0.1\ \text{s}^{-1}$. As the volume fraction exceeds this value, the viscosity rises to levels that cause practical difficulties in mixing. Accordingly, Mo/PBTTPA pastes with 35 vol% Mo represent good choices for realizing high electrical conductivity in a formulation with viscosity appropriate for screen printing.

The environmental/biological degradability of these materials represents an essential characteristic. Fig. 2a shows the DC electrical conductivity of Mo/PBTTPA as a function of time of

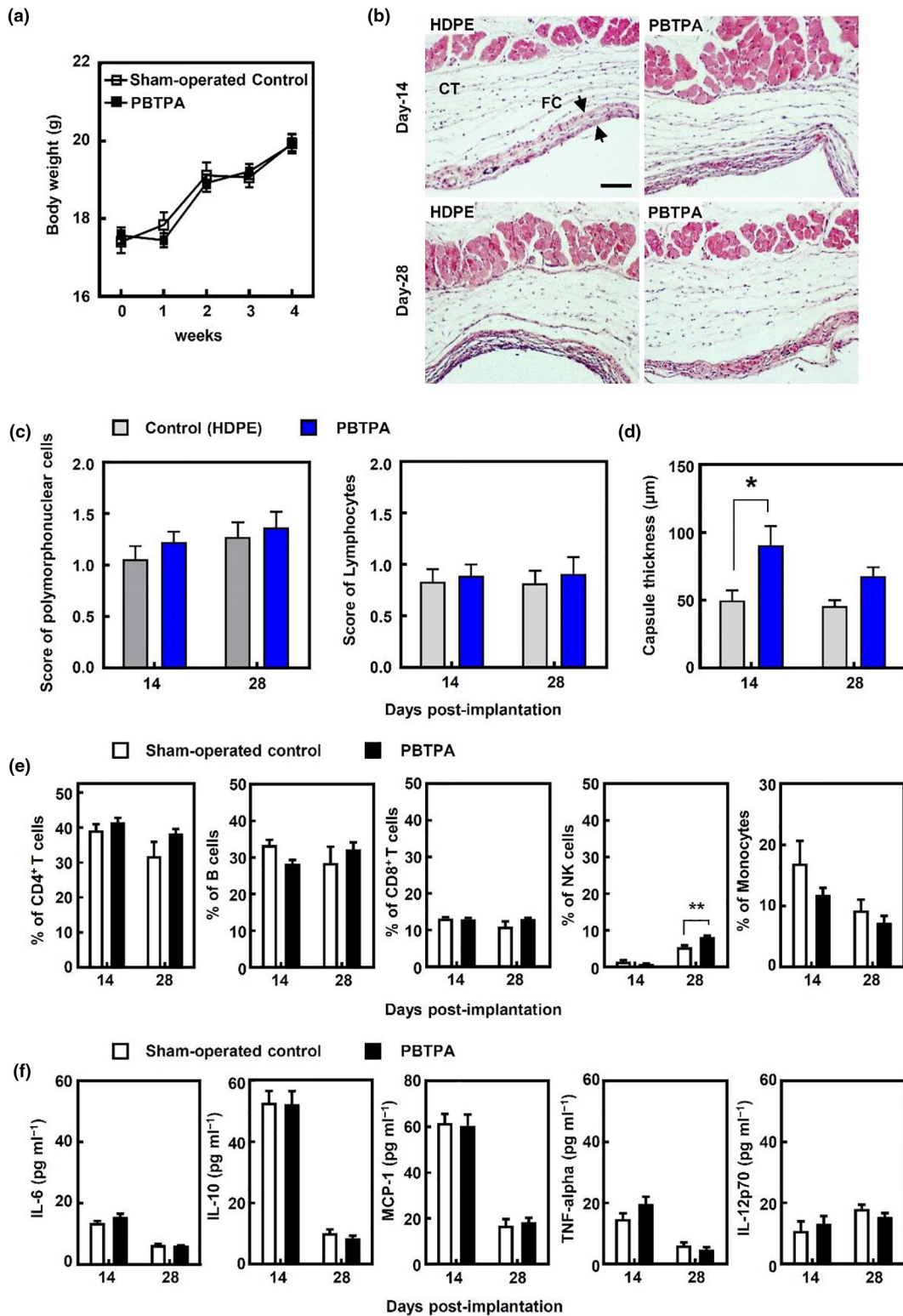
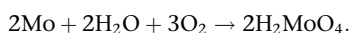


FIGURE 4

In vivo tests of biocompatibility of PBTPA. (a) Body weight of animals in each group (sham = 5, $n = 10$) measured weekly. (b) Optical micrograph of hematoxylin and eosin-stained slides of tissues surrounding the implants in the control (HDPE) and polyamide groups on days 14 and 28 post-implantation, respectively. The scale bar is 100 μm . (c) Histological evaluation of infiltrates of polymorphonuclear cells (PMN) and lymphocytes (CT, Connective tissue; FC, fibrous capsule). (d) Comparison of capsule thickness between HDPE and polyamide implant sites ($p < 0.05$). Two-tailed unpaired t test. (e) Frequency of cells in the peripheral blood from sham-operated mice ($n = 5$) and polyamide-implanted mice ($n = 10$) were assessed by flow cytometry (** $p < 0.01$). One-way analysis of variance Bonferroni's multiple comparison test. (f) Concentrations of systemic inflammatory cytokines (IL-6, IL-10, MCP-1, TNF-alpha, and IL-12p70) assessed by Cytometric Bead Array (CBA). (All data presented as the average and standard error of mean (SEM).)

immersion in various solutions, *i.e.* phosphate-buffered saline (PBS) 1X, PBS 10X, Hank's balanced salt solution (HBSS) and Bovine serum, at 37 °C. A relatively low resistance persists for over a week (Fig. S2). Additional results compare pastes formed with similar Mo volume fraction and other bioresorbable polymers (PLGA (75:25), PLGA (50:50), PLLA, and PCL), as in Fig. 2b. The hydrophobicity of the PBTPA is an important characteristic in this context; it can be controlled by adjusting the ratio of 4-pentenoic anhydride (4PA), 1,3,5-triallyl-1,3,5-triazine-2,4,6-(1H,3H,5H)-trione (TTT), and 1,4-butanedithiol since 1,4-butanedithiol contains the hydrophobic chain. Studies of polymers with two different ratios of 4PA, TTT, and 1,4-butanedithiol, *i.e.* 1:1:2.5 (PBTPA 1:1) and 1:4:7 (PBTPA 1:4), reveal the effects of hydrophilicity on dissolution. Specifically, the hydrophobic thin native oxide layer on the Mo microparticles improves their interactions with the polymer [28,29]. The rate of change in conductivity increases with hydrophilicity due to effects of water penetration, swelling and polymer degradation. Similar trends appear with other polymers. For PLGA, the molar ratio of lactide (less hydrophilic) to glycolide (more hydrophilic) defines the hydrophilicity. PLLA obtained from polymerization of L-lactide is semi-crystalline. PCL is also semi-crystalline, but compared to PLLA and PLGA, it degrades more slowly because it contains five hydrophobic $-\text{CH}_2$ moieties in its repeat unit. Because PBTPA is synthesized through *in situ* polymerization, the polymer homogeneously mixes with the Mo microparticles to yield uniform dispersions with enhanced interfacial adhesion between the Mo microparticles and PBTPA [30,31]. These features establish a compact conductive network, leading to high initial electrical conductivity, *i.e.* electrical conductivity before immersion in PBS solution. Also, the strong interfacial adhesion between Mo microparticles and PBTPA helps to prevent the permeation of water through the interfaces.

The dissolution processes can be studied by FTIR spectroscopy (Fig. 2c), using samples of neat PBTPA and Mo/PBTPA as a function of time of immersion in PBS solution at 37 °C. Normalizing the FTIR spectra to the peak at 1684 cm^{-1} , which is associated with a C=O stretching mode in the isocyanurate ring and the anhydride group, allows comparisons of the intensity of peaks related to the Mo microparticles. At low wavenumbers, the decreasing peaks in the range of $970\text{--}685\text{ cm}^{-1}$ correspond to Mo(VI), *i.e.* MoO_4^{2-} ions. Previous work suggests that the chemistry of dissolution of Mo in alkaline and neutral solutions (pH > 6) involves mainly $[\text{MoO}_4]^{2-}$ ions. As the pH decreases, the anion becomes protonated, giving the heptamolybdate $[\text{Mo}_7\text{O}_{24}]^{6-}$ ion at pH 5–6 and octamolybdate $[\text{Mo}_8\text{O}_{26}]^{4-}$ ion at pH 3–5 [32]. The overall chemistry is



Besides the C=O stretching peak and Mo (VI)-related vibrational bands, the characteristic peaks of PBTPA include the C–N stretching peak at 1462 cm^{-1} ; the C–O–C stretching bands at 1375 , 1335 , and 1288 cm^{-1} ; and the C–S stretching peak at 764 cm^{-1} as reported elsewhere [14]. The FTIR spectra without normalization show that the intensity of peaks related to the PBTPA also reduce with increasing time of dissolution (Fig. S3).

Scanning electron microscope (SEM) imaging reveals the microstructural changes that occur during the dissolution process (PBS solution at 37 °C), as in Fig. 2d and e. The dissolution of PBTPA involves breaking of the anhydride bond into carboxylic acids through hydrolysis of 4PA [33]. Since the PBTPA is more hydrophobic than the other bioresorbable polymers examined here, it establishes comparatively good contacts with the Mo microparticles, due to their hydrophobic native oxide (MoO_3), and it is resistant to water permeation [28,29]. Moreover, because the preparation of Mo/PBTPA involves *in situ* polymerization, the material exhibits good dispersion compared to pastes prepared by dissolving the polymer in solvent and mixing with Mo microparticles. For Mo/PLGA, the PBS solution penetrates along the interface between the Mo and PLGA, thereby initiating dissolution. The voids between the microparticles and the surrounding polymer increase in size over time, thereby reducing the conductivity. Here, the hydrophilic nature of PLGA leads to increased rates of dissolution in PBS solution (Fig. S5).

Fig. 3 summarizes various functional demonstrations of Mo/PBTPA as a conductive paste, with a Mo volume fraction of 0.35. Fig. 3a shows printed features with various feature sizes. Laser-milled (feature sizes between $100\text{ }\mu\text{m}$ and 3 mm) films of Kapton ($50\text{-}\mu\text{m}$ thickness) serve as screens for printing onto glass slides to form conductive lines ($100\text{ }\mu\text{m}$ ~ 3 mm width, $100\text{-}\mu\text{m}$ thickness, and 20- to 50-mm length). A small-scale LED (Digi-key Electronics, USA) placed between two adjacent lines and heated on a hot plate at $250\text{ }^\circ\text{C}$ serves as an indicator of electrical continuity. Fig. S6a shows various screen-printable serpentine lines ($400\text{ }\mu\text{m}$ ~ 1 mm line width), RF inductive coils ($800\text{-}\mu\text{m}$ widths for the conducting lines of the coil) and electrical connections with small LEDs. Fig. 3b presents images of an RF inductive coil (magnesium foil, thickness ~ $50\text{ }\mu\text{m}$, Solution Materials, LLC, USA, patterned by photolithography and etching in diluted hydrochloric acid HCl : DI water = 1:10) for wireless powering of an LED that is electrically connected to the coil by a small amount of Mo/PBTPA paste applied by hand and cured on a hot plate at $250\text{ }^\circ\text{C}$.

Printing a trace of Mo/PBTPA (1.5-mm width and $150\text{-}\mu\text{m}$ thickness) and heating it on a glass slide yield a simple test structure for monitoring changes in electrical properties during immersion in deionized (DI) water at $37\text{ }^\circ\text{C}$ (5-mm exposed length, defined by a well made of PDMS). Fig. S7 shows an image of the operation of an LED powered by current that passes through a trace of the Mo/PBTPA paste for as many as nine days before dissolution creates an open circuit. As another example, printed traces can serve as flexible strain sensors. Fig. 3c shows the structure, which consists of a line ($150\text{-}\mu\text{m}$ width, 30-mm length, $100\text{-}\mu\text{m}$ thickness) printed on a PDMS substrate (9:1, 20-mm width, 50-mm length 1.5-mm thickness). Cu wires embedded in 5-mm lengths of such lines provide a means to measure the change of resistance. After heating at $250\text{ }^\circ\text{C}$ on a hot plate, application of an encapsulating layer of PDMS (9:1, $200\text{ }\mu\text{m}$ thick) prevents delamination of the trace during stretching and bending. Here, controlled stretching (ATS100-150, AeroTech Inc., USA) of Mo/PBTPA lines on PDMS substrates yields corresponding changes in resistance, as expected. Fig. 3d summarizes the results of the application of uniaxial strain (3%, 5%, and 7%) over 10 cycles using a stretching instrument (ATS100-150,

AeroTech Inc., USA). As the sample is stretched, the inter-particle distance increases, leading to the destruction of parts of the conductive network, thereby increasing the resistance. When the sample reverts to its unstrained state, the conductive network reforms, and the resistance recovers to the initial value [34,35]. The data show that these changes are reversible, to within experimental error, and that the behavior is therefore recoverable for modest numbers of cycles. Here, the behavior at high strain rates likely arises, at least partly, from the viscoelasticity of the polymer [36]. Fig. 3e shows the change in resistance as a function of stretching and releasing to a strain of 5%. The gauge factor is ~ 20 , which is reasonable for composites of this type [37–40]. Such devices can be used for motion sensing, as demonstrated in the context of bending a finger in Fig. S8. A slightly different embodiment, as in Fig. S9a, yields a pressure sensor through the use of a curved PDMS substrate (radius of curvature = 120 mm). The data in Fig. 3f summarize the pressure changes measured by loading masses on top of such a device (US pennies, at 2.5 g per coin) using digital multimeter (NI USB-4065, National Instruments, USA). Fig. S9b presents images that show the gradual flattening of the PDMS with increasing mass.

The biocompatibility of Mo and PBTPA is essential for applications of Mo/PBTPA in temporary implants. Previous studies of the response of human cells exposed to Mo particles reveal no significant cytotoxicity for concentrations up to 800 $\mu\text{g}/\text{ml}$ of Mo [41]. From a practical standpoint, 800 $\mu\text{g}/\text{ml}$ is a high concentration compared to those expected from the dissolution of Mo/PBTPA traces. For instance, *ca.* 1.5 cm of the Mo/PBTPA trace (150- μm width, 100- μm thickness) would be compatible with this upper limit of concentration (800 $\mu\text{g}/\text{ml}$) in 1 ml of biofluid. Furthermore, in general, no significant cytotoxicity up to 800 $\mu\text{g}/\text{ml}$ indicates its excellent biocompatibility [42,43]. Investigations of PBTPA 1:4 summarized here focus on small samples inserted subcutaneously into individual Balb/c mice, along with controls of high-density polyethylene (HDPE, FDA-approved nontoxic control), to examine foreign body reactions. A group of mice subjected to the similar surgery but without implants serves as an additional control (Sham-operated control). The data in Fig. 4a indicate that the changes in body weight observed in sham-operated control and PBTPA-implanted mice are similar. Following implantation, mice behaved normally with no substantial skin necrosis or swelling for up to 28 days (Fig. S10).

Histological observation provides information on the presence of polymorphonuclear leukocytes (PMNs), lymphocytes, and fibrous capsule formation in the surrounding tissues. Hematoxylin and Eosin (H&E)-stained sections of implant sites surrounding tissues show comparable levels of immune cell infiltration between HDPE- and polyanhydride-implanted tissues on days 14 and 28 (Figs. 4b and S11). The number of PMNs and lymphocytes surrounding the implanted sites is comparable between HDPE- and polyanhydride-implanted tissues (Fig. 4c). Slightly elevated fibrosis, measured as capsule thickness, can be observed in mice implanted with polyanhydrides (Fig. 4d). These fibrous capsules appear 14 days post-implantation, but return to a range comparable to HDPE on the 28th day. These data suggest that there may be a mild foreign body reaction immediately following implantation but that this reaction later resolves itself. No significant changes in the frequency of immune cell subpop-

ulations (CD4+ T cells, CD8+ T cells, B cells, and monocytes) are noted in the peripheral blood (Fig. 4e), suggesting that polyanhydrides do not cause strong immunogenicity following subcutaneous implantation. A slightly increased percentage of NK cells appears on day 28 in the blood, but this increase is not present in the spleen (Figs. S12b and 12c). Furthermore, slight changes of B and CD8+ T cell percentage occur after 14 days of polyanhydride implantation, but these changes neither persist nor cause significant changes in total immune numbers (Fig. S12a). The serum levels of inflammatory cytokines, IL-10, IL-6, TNF-alpha, and IL-12p70 in the polyanhydride group are comparable to those in the sham-operated control group 14 and 28 days post-implantation (Fig. 4f). Collectively, these data demonstrate that although mice implanted with polyanhydride show some temporary changes in immune cell populations, these changes do not generate any visible side effects.

Conclusion

The materials described here provide the basis for water-soluble conductive inks that offer stable operation over extended periods of immersion in aqueous environments. Fundamental studies and comparative assessments with other paste formulations establish the key considerations in materials design and the relationship to electrical and physical properties. Patterning of conductive traces formed with these materials and integration of them into bioresorbable electronic devices illustrate their suitability for use in circuits, interconnects, inductive antennas, strain gauges, and pressure sensors. Moreover, *in vivo* immunochemistry tests verify the biocompatibility of the Mo/PBTPA paste and its dissolution products, indicating broad potential for application in biomedical devices.

Materials and methods

Synthesis of polyanhydrides

Mixing 4-pentenoic anhydride (4PA), 1,3,5-triallyl-1,3,5-triazine-2,4,6(1H,3H,5H)-trione (TTT), and 1,4-butanedithiol with 2,2-dimethoxy-2-phenylacetophenone as a photoinitiator, followed by illumination with ultraviolet (UV) light (364 nm) for an hour yielded poly butanedithiol 1,3,5-triallyl-1,3,5-triazine-2,4,6(1H,3H,5H)-trione pentenoic anhydride (PBTPA). The two formulations of PBTPA used different molar ratios between 4PA, TTT, and 1,4-butanedithiol; 1:4:7 (PBTPA 1:4) and 1:1:2.5 (PBTPA 1:1), respectively. All chemicals were purchased from Sigma-Aldrich Co. (USA).

Preparation of bioresorbable conductive paste

Dispersing molybdenum (Mo) microparticles with diameters between 1 and 5 μm (Sigma-Aldrich Co., USA) in PBTPA formed the bioresorbable conductive paste. The volume fraction of Mo in PBTPA ranged from 0.21 to 0.35, corresponding to 2.5, 3, 3.5, 4, 4.5, and 5 g of Mo to 1 g of PBTPA. Illumination with UV light initiated the polymerization. Subsequent thermal curing and densification yielded a conductive network *via* small deformations in the polymer matrix and cross-linking of polymer not fully cured by UV light. Measurements with an impedance analyzer (Solartron 1260, Solartron Analytical, Farnborough, UK) yielded the AC conductivity (in the frequency

range from 100 kHz to 1 MHz) of six different concentrations of Mo/PBTPA. A rheometer (MCR 302, Anton Paar, Gratz Austria) allowed for evaluation of the dynamic viscosity (*i.e.* absolute viscosity, or shear viscosity, defined as the ratio of shear stress to shear rate as measured by a rheometer [44–47]) of these materials. Formation of pastes with other bioresorbable polymers, *i.e.* poly(lactide-co-glycolide) (PLGA), poly(L-lactide) (PLLA), and polycaprolactone (PCL), involved dissolving the polymer in ethyl acetate and dispersing the Mo microparticles into the resulting solution. Pastes formed with tungsten (W), zinc (Zn), and iron (Fe) served as additional points of comparison, where the characteristic sizes of the corresponding microparticles were all less than 10 μm . All chemicals including bioresorbable polymers and metal microparticles were purchased from Sigma-Aldrich Co. (USA).

Dissolution tests

Casting six different kinds of bioresorbable conductive paste (PBTPA 1:4, PBTPA 1:1, PLGA 75:25, PLGA 50:50, PLLA, and PCL) on glass slides and curing them by exposure to UV light for one hour followed by heat treatment produced solid samples (25 mm \times 25 mm, *ca.* 190 μm thickness). Immersion studies involved four different solutions, *i.e.* phosphate-buffered saline (PBS) 1X, 10X (Gibco), Hank's Balanced Salt Solution (HBSS, Gibco), and fetal bovine serum (Gibco), all at 37 °C. Measurements using an FTIR spectrometer (Nexus 870, Thermo Nicolet Co., Madison, WI, USA) and a scanning electron microscope (SEM, Hitachi SU8030, Hitachi, Yokohama, Japan) revealed the dissolution mechanisms, in terms of the chemical changes in the polymer and the morphological changes of the pastes, respectively.

Application examples

Laser-milled (feature sizes between 100 μm and 3 mm) films of polyimide (Kapton, 50- μm thickness) served as masks for formation of conductive lines (100 μm \sim 3 mm width, 100- μm thickness, and 20- to 50-mm length) by casting Mo/PBTPA paste with a blade, onto a glass slide. A small-scale LED (Digi-key Electronics, USA) placed between two lines and sintered on a hot plate at 250 °C provided a visual indicator of electrical continuity. A substrate of polydimethylsiloxane (PDMS, 9:1, 1.5-mm thickness, Sylgard 184, Dow Corning, USA) supported the bioresorbable wireless circuit, formed with an RF coil created by cutting a piece of Mg foil (50- μm thickness). A Cu wire (Goodfellow Co., USA) electrically bridged the start and end points of the coils. Applying the Mo/PBTPA paste baking on a hot plate at 250 °C for 30 min established an electrical interconnection. Placing the integrated device in proximity to the primary coil allowed operation of the LED with radio frequency wireless power at 15 MHz.

Functional dissolution tests

A PDMS well structure (Sylgard 184, Dow Corning, USA) placed on a conductive PBTPA line and sealed by additional PDMS material around the contacting interface was filled with distilled (DI) water and covered by a slab of PDMS. The samples were stored in an oven at 37 °C. A voltage of 100 mV was applied

(Agilent E3631A, USA) during the degradation of the Mo/PBTPA paste.

Fabrication and testing of strain and pressure sensors

Fabrication of the strain sensor began with preparation of a flexible substrate (9:1 PDMS, 20-mm width, 30-mm length, and 1.5-mm thickness). Screen printing defined features of Mo/PBTPA paste (150- μm width, 30-mm length, and 100- μm thickness). Cu wires embedded in 5-mm lengths at the ends of the lines of Mo/PBTPA allowed measurements of changes in resistance. Sintering at 250 °C on a hot plate completed the process. Finally, PDMS (9:1, 200 μm thick) cast on top of the entire device prevented delamination of the Mo/PBTPA paste from the flexible substrate during stretching and bending. The stretching test involved the application of uniaxial strain (3%, 5%, and 7%) over 10 cycles using a stretching instrument (ATS100-150, Aero-Tech Inc., USA). Fabrication of the pressure sensor began with preparation of a curved substrate (9:1 PDMS, 20-mm width, 50-mm length 1.5-mm thickness, and 150-mm curled radius) by casting on a round surface. The remaining processing steps followed those for the strain sensor. The change in resistance with applied load was measured using a digital multimeter.

In vivo biocompatibility tests

Female Balb/c mice (6–8 weeks) were purchased from Narabio (Seoul, Korea). All procedures were approved by Korea University Institutional Animal Care & Use Committee (KUIACUC-2013–93). Mice were anesthetized with 30 mg/kg zolazepam hydroxide (Zoletil 50; Virbac, Sao Paulo, Brazil) and 10 mg/kg xylazine hydroxide (Rumpun; Bayer, Shawnee Mission, KS), high-density polyethylene (HDPE, nontoxic control), and polyanhydrides were implanted subcutaneously through dorsal incision. Following 14 or 28 days of implantation, the mice were sacrificed for histology. Tissue samples were fixed in 10% neutral buffered formalin, embedded in paraffin, sectioned, and stained with Hematoxylin and Eosin (H&E) for histological analysis. Polymorphonuclear cells and lymphocytes were identified by morphology from at least three distinct regions by 400 \times fields per samples. Histological scores were assessed as reported earlier. Five random locations were chosen for the capsule thickness measurements from optical micrographs at 10 \times magnification. Cell suspensions were blocked with anti-CD16/CD32 mAbs (clone 2,4G2) for 10 min and then incubated with the following antibodies for 20 min at 4 °C. Fluorescently conjugated mAbs against CD3e (145-2C11), CD8 (53-6.7), CD4 (GK1.5), CD19 (1D3), CD49b (Dx5), CD11b (M1/70), CD11c (N418), and Ly-6G (Gr-1) were purchased from eBioscience (San Diego, CA, USA). Populations were described as the following: CD4+ T cells (CD3e + CD4+), CD8+ T cells (CD3e + CD8+), B cells (CD3e-CD19+), NK cells (CD3e-Dx5+), monocytes (CD11b + Ly-6G-), and neutrophils (CD11b + Ly-6G+). Flow cytometry was performed using FACSCantoII (BD Biosciences, San Diego, CA, USA), and data were analyzed using FlowJo software (Three Star, Ashland, OR, USA). Serum concentrations of IL-6, IL-10, MCP-1, IFN- γ , TNF, and IL-12p70 were measured using a CBA Mouse Inflammation Kit (BD Biosciences, San Diego, CA, USA), according to the manufacturer's instructions.

Acknowledgments

This work was supported by Basic Science Research Program through the National Research Foundation of Korea (NRF) funded by the Ministry of Science, ICT & Future Planning (NRF-2017R1A2B3004828 and NRF-2013M3A9D3045719) awarded to K.-M. Lee.

Appendix A. Supplementary data

Supplementary data associated with this article can be found, in the online version, at <https://doi.org/10.1016/j.mattod.2017.12.005>.

References

- [1] S.-W. Hwang et al., *Adv. Funct. Mater.* 23 (2013) 4087.
- [2] K.K. Fu et al., *Chem. Mater.* 28 (2016) 3527.
- [3] D.-H. Kim et al., *Nat. Mater.* 9 (2010) 511.
- [4] H. Acar et al., *Adv. Funct. Mater.* 24 (2014) 4135.
- [5] C.M. Boutry et al., *Adv. Mater.* 27 (2015) 6954.
- [6] H. Bae et al., *Sci. Rep.* 6 (2016) 38324.
- [7] M. Irimia-Vladu et al., *Adv. Funct. Mater.* 20 (2010) 4069.
- [8] K. Fu et al., *Nano Lett.* 15 (2015) 4664.
- [9] C.J. Bettinger, Z. Bao, *Adv. Mater.* 22 (2010) 651.
- [10] S.-W. Hwang et al. J.A. Rogers, *Science* 337 (2012) 1640.
- [11] K. Fu et al., *Adv. Energy Mater.* 6 (2016) 1502496.
- [12] C.H. Lee et al., *Adv. Funct. Mater.* 25 (2015) 5100.
- [13] C. Dagdeviren et al., *Small* 9 (2013) 3398.
- [14] S.-K. Kang et al., *Nature* 530 (2016) 71.
- [15] S.-W. Hwang et al., *Nano Lett.* 15 (2015) 2801.
- [16] X. Huang et al., *Adv. Mater.* 26 (2014) 7371.
- [17] Y.K. Lee et al., *Adv. Mater.* 29 (2017) 1702665.
- [18] M. Uygun, M.A. Tasdelen, Y. Yagci, *Macromol. Chem. Phys.* 211 (2010) 103.
- [19] H. Deng et al., *Polymer* 50 (2009) 3747.
- [20] I. Alig et al., *Phys. Stat. Sol. (b)* 244 (2007) 4223.
- [21] G. Wu et al., *J. Appl. Phys.* 88 (2000) 1480.
- [22] S.J. Babinec et al., *Adv. Mater.* 12 (2000) 1823.
- [23] E.P. Mamunya, V.V. Davidenko, E.V. Lebedev, *Polym. Compos.* 16 (1995) 319.
- [24] D.C. Tsui et al., *Surf. Sci.* 73 (1978) 419.
- [25] N.B. Mansour et al., *Appl. Surf. Sci.* 337 (2015) 158.
- [26] R. Tlili, M. Khelil, et al., *Ceram. Int.* 42 (2016) 11256.
- [27] H.P. Wu et al., *Comp. Sci. Tech.* 67 (2007) 1116.
- [28] S. Ashraf et al., *J. Mater. Chem.* 16 (2006) 3575.
- [29] K. Hong et al., *J. Electrochem. Soc.* 156 (2009) H648.
- [30] Y. Habibi, S. Benali, P. Dubois, In situ polymerization of bionanocomposites, in: O. Kristiina, M. Aji, P.B. Alexander (Eds.), *Handbook Of Green Materials: Processing Technologies, Properties and Applications*, World Scientific, Singapore, 2014, pp. 69–88.
- [31] X.-L. Xie et al., Polymer-magnesium hydroxide nanocomposites by emulsion polymerization, in: V. Mittal (Ed.), *Polymer Nanocomposites by Emulsion and Suspension Polymerization*, Royal Society of Chemistry, London, 2011, pp. 180–197.
- [32] J. Aveston, E.W. Anacker, J.S. Johnson, *Inorg. Chem.* 3 (1964) 735.
- [33] A. Göpferich, J. Tessmar, *Adv. Drug. Deliv. Rev.* 54 (2002) 911.
- [34] X. Cao et al., *Polymer* 112 (2017) 1.
- [35] K.P. Sau, T.K. Chaki, D. Khastgir, *Compos. A* 29A (1998) 363.
- [36] M. Amjadi et al., *Adv. Funct. Mater.* 26 (2016) 1678.
- [37] N. Lu et al., *Adv. Funct. Mater.* 22 (2012) 4044.
- [38] Y.R. Jeong et al., *Adv. Funct. Mater.* 25 (2015) 4228.
- [39] C. Mattmann, F. Clemens, G. Tröster, *Sensors* 8 (2008) 3719.
- [40] C.S. Boland et al., *ACS Nano* 8 (2014) 8819.
- [41] M.J. Akhtar et al., *J. Colloid. Interface Sci.* 457 (2015) 370.
- [42] X. Wang et al., *Int. J. Clin. Exp. Pathol.* 7 (2014) 1337.
- [43] K. Shin et al., *Nat. Commun.* 8 (2017) 15807.
- [44] M. Dietze, M. Es-Souni, *Sens. Actuators A Phys.* 143 (2008) 329.
- [45] P. Ried et al., *J. Eur. Ceram. Soc.* 28 (2008) 1801.
- [46] D.-Y. Shin, Y. Lee, C.H. Kim, *Thin Solid Films* 517 (2009) 6112.
- [47] J.W. Phair, A.F.-J. Kaiser, *Ann. Trans. Nordic Rheol. Soc.* 17 (2009).